Preprint version of:
Feliu-Talegon, D., Nekoo, S. R., Suarez, A., Acosta, J. A. & Ollero, A. ROBOT 2022, Accepted.. Fully Coupled Six-DoF Nonlinear Suboptimal Control of a Quadrotor: Application to Variable-Pitch Rotor Design. In ROBOT2022: Fifth Iberian Robotics Conference. (Accepted)

Modeling and Under-actuated Control of Stabilization Before Take-off Phase for Flapping-wing Robots

Daniel Feliu-Talegon*, Saeed Rafee Nekoo, Alejandro Suarez, Jose Angel Acosta, and Anibal Ollero

The GRVC Robotics Lab., Departamento de Ingeniería de Sistemas y Automática Escuela Técnica Superior de Ingeniería, Universidad de Sevilla, Seville, Spain
*Corresponding Author: danielfeliu@us.es

Abstract. This work studies a stabilization problem of flapping-wing flying robots (FWFRs) before a take-off phase while a robot is on a branch. The claw of the FWFR grasps the branch with enough friction to hold the system steady in a stationary condition. Before the take-off, the claw opens itself and the friction between the claw and branch vanishes. At that moment, the mechanical model turns into an under-actuated multi-link (serial configuration) robotic system where the first joint can rotate freely without any friction as opposed to rotation. The stabilization and balancing are the crucial tasks before take-off. This work explores a new methodology to control an under-actuated lightweight manipulator for its future adaptation to FWFR to improve the stabilization performance before take-off. The setup tries to mimic the birds with two-link legs, a body link, and 2-DoF (degrees of freedom) arms, being all active links except the first passive one. In contrast to common arms, the lightweight-design restriction limits the frame size and requires micromotors. With all of these constraints, control design is a challenge, hence, the system is categorized: a) the leg subsystem (under-actuated), including the two first links, and b) the body and arm subsystem (fully actuated) with the rest of links. The fully-actuated links are controlled by feedback linearization and the under-actuated part with active disturbance rejection control (ADRC) for estimation and rejection of the coupling between both subsystems. The mechanical design, modeling, and control of the proposed system are reported in this work. Experimental results have been also proposed to present a proof of concept for this modeling and control approach.

Keywords: Flapping-wing robot, Under-actuated, Robust, Take-off, Aerial robot.

1 Introduction

The operation of ornithopters, or flapping-wing flying robots (FWFRs), with manipulation capabilities, includes several phases such as launching, flapping flight, possible gliding, perching/landing, stabilization after perching, sampling/manipulation, and take-off again. The initial launching phase is usually done by hand for small to medium scale birds [1–3]; and in some cases by a special external launcher system [4], or self-launching mechanisms (take-off system) [5, 6]. The robot birds for launching must be posed in a proper position to facilitate the take-off maneuver which defines the initial

condition of the robot. Hoff and Kim used a launching mechanism to gain similar initial conditions for finding a data-driven model [4]. Afakh et al. developed a flapping robot that could fly from the ground without assisting mechanism [5]. The robot was placed in a high pitch angle pose to enable a successful take-off from the ground. The problem of the take-off from a branch after manipulation or completing a task requires the same condition. The FWFR must be in a proper pose with a high pitch angle. Here in this work, the stabilization of the robot bird before the take-off is investigated to put the robot in a desired position/orientation. Considering the take-off after perching on a branch using a mechanical claw with enough friction, it is assumed that the bird does not rotate or slide on the branch when the claw is closed, and it can hold its body steadily with a fixed pose. Reopening the claw removes the friction, and the FWFR will act on the branch like an inverted pendulum (an under-actuated model) for a split of a second before take-off. Here in this work, an underactuated mechanical system is modeled to analyze the problem and control the trajectory of the body before flying again. This is important since the perching might not pose the body in the desired configuration for take-off. Then the leg moves the body based on the designed trajectory.

Inverted pendulums are challenging models because of under-actuation conditions. Under-actuation imposes two difficulties to the system: controllability problem and reduced range of convergence in comparison with fully actuated mechanisms [7, 8]. Previous works [9] and [10] study the nonlinear control problem of underactuated systems considering static friction at its first passive joint to explore the possibility to perform manipulation with FWFR once the system is perched. This work focuses on a new methodology to control an under-actuated lightweight manipulator that emulates the behavior of a bird on the branch just before the take-off phase. The main difference with the mentioned works is that we consider that the claw is opened and the friction at this first passive joint has vanished which means that the first passive joint can rotate freely without any friction as opposed to the rotation. The weight limits the configuration, and geometry and leads us to use micromotors and very lightweight materials. For example, in [11] a new sensor system is developed that emulates the beak's bird to allow FWFR to interact with the environment. Then, the mentioned work is devoted to two tasks: a) to maintain the equilibrium of the body while perching and b) to control the force interaction with the environment. Although, there are various methods and available results for under-actuated systems, the hard constraints imposed by nature to mimic the anatomy of birds, make necessary the exploration of the most appropriate control techniques.

The actual system behaves similarly to that of the acrobot [12]. The setup is a two-DoF under-actuated robot that replicates the human acrobat who hangs from a rope and tries to balance. The control of n-link under-actuated manipulators with a passive first link has been investigated in the last decades as in e.g. [13], and [14]. Unlike [9] and [10], there is no static friction at the base of the manipulator because just before the take-off, the claw opens itself and the friction between the claw and branch vanishes. However, manipulation with under-actuated systems has been rarely investigated due to its difficulty, and therefore it is still an open challenge. Our prototype is a multi-link planar under-actuated robot with a passive first link. A first approximation to control is the decoupling of the actuated and under-actuated systems. The first subsystem is under-

actuated and composed of a passive first link and an active second one (similar to an acrobot). The second subsystem is composed of the remaining fully-actuated links. On the one hand, for the well-known fully-actuated subsystem state-feedback linearization control technique has been employed [15–17]. On the other hand, for the acrobot-like subsystem, due to the high uncertainty coming from the coupling term and the limited implementation, robust control has been used, the method is so-called active disturbance rejection control (ADRC).

The ADRC inherits the conventional linear controllers, enhanced by nonlinear feedback and robustness obtained by the addition of additional fictitious state variable [18, 19]. The active disturbance rejection control is a powerful tool for under-actuated mechanical systems especially in experimentation [20, 21]. Uncertainty in parameters, unknown friction values in the model, time-varying control, and unknown torque load motivated the application of the ADRC [21]. Ma et al. used a data-driven type of ADRC for a crane pendulum model using flat output [22]. Sparse regression was employed to find the interaction between the states and the flat output. Moreover, a recent theoretical breakthrough in [23] allows using the Lyapunov theory to analyze stability in cascade nonlinear systems and hence, is very suitable for the work presented here. More details are available in [24] for flatness and the generalized proportional integral (GPI) observers; [25] for academic and industrial engineering applications; and in particular works in [23, 26] demonstrated that this method suits well for under-actuated systems.

The main contribution of this work is to present a model for the under-actuated state of a flapping wing robot, right before take-off from a branch, and control the trajectory of the system using feedback linearization and an active disturbance rejection approach. The rest of the paper is organized as follows. Section II presents the description and model of the system. Section III presents the strategy of the proposed control. Section IV describes the actual prototype (IV-A), simulation results (IV-B), and experimental data (IV-C). Concluding remarks are presented in Section V.

2 Description and modeling of the system

As a first approach, we consider the study of a system composed of an actuated leg, a body, and an actuated arm in a two-dimensional space, considering that the real 3D system will be made with a pair of them. Figure 1 left depicts a scheme of the system case of study. The system is equipped with n-links ($i = 1, \ldots, n$) of length l_i, and masses concentrated at their tips m_i. The first link has a passive joint at its base whereas the other joints are active. The torques provided by the motors in the active joints are Γ_i. Figure 1.a depicts a schematic of the system where θ_i are the angular positions of the joints. The control objective is to follow a trajectory with the tip in order to achieve a desired posture with the system while maintaining the equilibrium of the system. This is important to perform lately the take-off maneuver. As it was aforementioned, we split the system into two subsystems: the first subsystem $\theta_1 - \theta_2$ (similar to an acrobot), and the second subsystem defined through the remaining fully-actuated links. Let us now derive the dynamic model of the underactuated manipulator with a single passive joint at its base. To simplify the approach n-link fully-actuated mechanism is treated as the only one whose dynamics are all concentrated at the center of mass of those three links. Thus,

let $q = [\theta_1, \theta_2, ..., \theta_n]^T \in \mathbb{R}^n$ denotes the the joint angles in generalized coordinates, and $U = [0, \Gamma_2, \Gamma_3, ..., \Gamma_n]^T \in \mathbb{R}^n$ the control input vector. Then, the Lagrange dynamics of the n-link underactuated robot manipulator can be expressed as

$$M(q)\ddot{q} + C(q,\dot{q})\dot{q} + G(q) = U, \tag{1}$$

where $M(q) \in \mathbb{R}^{n\times n}$ is a symmetric positive definite inertia matrix; $C(q,\dot{q}) \in \mathbb{R}^{n\times n}$ is the Coriolis and centrifugal forces matrix; and $G(q) \in \mathbb{R}^n$ is the gravity force vector. Following the subsystem approach described above, the equation (1) can be rewritten in two blocks in an obvious way as follows

$$\begin{bmatrix} M_{12} & M_c \\ M_c^T & M_{3n} \end{bmatrix} \begin{bmatrix} \ddot{q}_{12} \\ \ddot{q}_{3n} \end{bmatrix} + \begin{bmatrix} C_{12} & C_{c1} \\ C_{c2} & C_{3n} \end{bmatrix} \begin{bmatrix} \dot{q}_{12} \\ \dot{q}_{3n} \end{bmatrix} \begin{bmatrix} g_{12} \\ g_{3n} \end{bmatrix} = \tau,$$

where $q_{12} = [\theta_1, \theta_2]^T$, $q_{3n} = [\theta_3, ..., \theta_n]^T$, $\tau := [\tau_{12}, \tau_{3n}]^T$ with $\tau_{12} = [0, \Gamma_2]^T$, $\tau_{3n} = [\Gamma_3, ..., \Gamma_n]^T$.

3 Control strategy

In this section, a cascade control scheme is derived from each subsystem separately. The proposed control scheme divides the system into two parts: 1) control of the underactuated part of the system (first subsystem $\theta_1 - \theta_2$) using an active disturbance rejection control technique and a GPI Observer to estimate the coupling between the two subsystems and the unmodelled dynamics and 2) control the trajectory of the remaining fully actuated part using feedback linearization. Figure 1.b shows a simplified scheme of the proposed methodology.

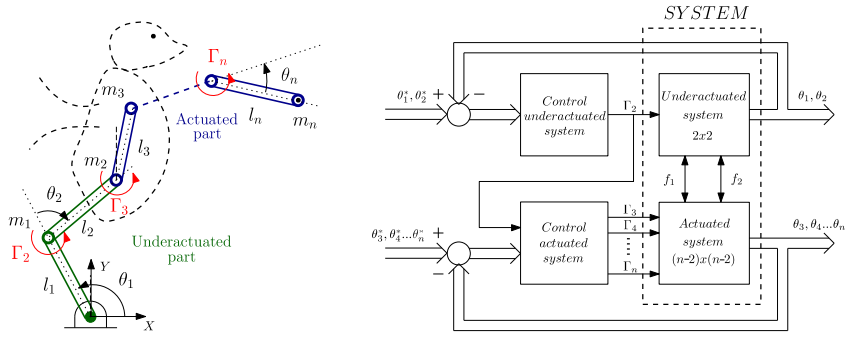

(a) (b)

Fig. 1 a) Schematic of the system and b) general control scheme.

3.1 Underactuated subsystem

The underactuated subsystem consists of a multivariable non-linear time-invariant system, which has two outputs θ_1, θ_2 and one input Γ_2. Recall that the proposed control technique is the ADRC. The idea is to consider the influence of the other subsystem as

an external disturbance that can be estimated and approximately canceled in the feedback loop. Notice that this can be done because the other subsystem is fully actuated. The dynamics of this subsystem becomes

$$M_{12}\ddot{q}_{12} + C_{12}\dot{q}_{12} + g_{12} + F(q_k, \dot{q}_k, \ddot{q}_k) = 0, \quad k = 1, ..., 3, \tag{2}$$

where $F(\cdot)$ is the coupling term between both subsystems.

Remark 1. It is important to highlight that the disturbance $F(\cdot)$ depends on all the angular coordinates, but only on the first and second derivatives of the angular coordinates of the other subsystem, which is crucial for its implementation.

We follow the standard approach to derive the ADRC controller. To this end, we first linearize the system around an equilibrium point $\theta_1 = \theta_{10}$, $\theta_2 = \theta_{20}$, $\dot{\theta}_1 = 0$ and $\dot{\theta}_2 = 0$. The incremental variables are defined as $\theta_{1\delta} = \theta_1 - \theta_{10}$, $\theta_{2\delta} = \theta_2 - \theta_{20}$, $\dot{\theta}_{1\delta} = \dot{\theta}_1$ and $\dot{\theta}_{2\delta} = \dot{\theta}_2$.

$$a_{11}\ddot{\theta}_{1\delta} + a_{12}\ddot{\theta}_{2\delta} + c_1\theta_{1\delta} + c_2\theta_{2\delta} + f_1 = 0, \tag{3}$$
$$a_{21}\ddot{\theta}_{1\delta} + a_{22}\ddot{\theta}_{2\delta} + c_3\theta_{1\delta} + c_4\theta_{2\delta} + f_2 = \Gamma_{2\delta}. \tag{4}$$

The functions f_1 and f_2 are considered as disturbances prompted for the other subsystem that can be eliminated. Thus, for the linearized system it is straightforward to see that the output defined as $y := a_{11}\theta_{1\delta} + a_{12}\theta_{2\delta}$ is flat. From equation (3) and the flat output, it can be obtained

$$\begin{pmatrix} \theta_{1\delta} \\ \theta_{2\delta} \end{pmatrix} = \begin{pmatrix} a_{11} & a_{12} \\ -c_1 & -c_2 \end{pmatrix}^{-1} \begin{pmatrix} y \\ \ddot{y} \end{pmatrix}, \tag{5}$$

and therefore, the input-to-flat output relation yields

$$\Gamma_{2\delta} = \underbrace{\frac{a_{21}\cdot a_{12} - a_{22}\cdot a_{11}}{a_{11}\cdot c_2 - a_{12}\cdot c_1}}_{K_0} y^{(4)} + \underline{\xi}(t), \tag{6}$$

with K_0 a control gain and $\underline{\xi}(t)$ depending on the flat output, y, and its first and second derivatives. Thus, with the ADRC methodology (e.g [26] and [27]) we obtain the following simplified input-output model of the system

$$y^{(4)} = \frac{1}{K_0}\Gamma_{2\delta} + \xi(t), \tag{7}$$

where $\xi(t)$ represents some neglected internal dynamics and disturbances.

GPI Observer The GPI observer is a breakthrough of state observers that can simultaneously estimate the states and their time derivatives and the total disturbance of the

system. The consecutive time derivatives of the flat output are computed using the following GPI observer

$$\begin{aligned}
\dot{\hat{y}}_0 &= \hat{y}_1 + l_4(y-\hat{y}_0),\\
\dot{\hat{y}}_1 &= \hat{y}_2 + l_3(y-\hat{y}_0),\\
\dot{\hat{y}}_2 &= \hat{y}_3 + l_2(y-\hat{y}_0),\\
\dot{\hat{y}}_3 &= \frac{\Gamma_{2\delta}}{K_0} + l_1(y-\hat{y}_0) + z,\\
\dot{z} &= l_0(y-\hat{y}_0),
\end{aligned}$$

allowing to estimate the perturbation terms $\xi(t)$ algebraically via the state of the observer $z(t)$. Additionally, from (7) and defining the observation error as $e_0 := y-\hat{y}_0$, the coefficients of the GPI observer, l_i, are chosen so that the reconstruction error dynamics becomes

$$e_0^{(5)} + l_4 e_0^{(4)} + l_3 e_0^{(3)} + l_2 \ddot{e}_0 + l_1 \dot{e}_0 + l_0 e_0 = \dot{\xi}(t), \tag{8}$$

and such that its associated polynomial $p_o(s) = s^5 + l_4 s^4 + l_3 s^3 + l_2 s^2 + l_1 s + l_0$ is Hurwitz, rendering an exponentially decreasing estimation error for any bounded $\dot{\xi}(t)$. To ease its tuning the polynomial can be defined in normal form as $p_o(s) = (s^2 + 2\zeta_o \omega_o s + \omega_o^2)^2 (s + T_o)$.

Active Disturbance Rejection Controller Given the flat output, its derivatives, and the estimation of the disturbance term $z(t)$, the GPI-ADRC scheme to track the output reference trajectory $y^*(t)$ is defined as

$$\frac{\Gamma_{2\delta}(t)}{K_0} = y^{*(4)}(t) - \gamma_3(\hat{y}^{(3)} - y^{*(3)}(t)) - \gamma_2(\ddot{\hat{y}} - \ddot{y}^*(t)) - \gamma_1(\dot{\hat{y}} - \dot{y}^*(t)) - \gamma_0(\hat{y} - y^*(t)) - z(t),$$

that upon defining the tracking error as $e_c := \hat{y} - y^*$, it forces a tracking error dynamics given by

$$e_c^{(4)} + \gamma_3 e_c^{(3)} + \gamma_2 \ddot{e}_c + \gamma_1 \dot{e}_c + \gamma_0 e_c = \xi(t) - z(t), \tag{9}$$

where the linear controller gains, γ_i, are set by using a fourth-order Hurwitz polynomial $p_c(s) = s^4 + \gamma_3 s^3 + \gamma_2 s^2 + \gamma_1 s + \gamma_0$, or in normal form $p_c(s) = (s^2 + 2\zeta_c \omega_c s + \omega_c^2)^2$, such that the closed-loop tracking error e_c converges exponentially to zero provided that $\xi(t) - z(t)$ tends to zero. The analysis of the stability and tracking of ADRC with extended observers for nonlinear time-varying uncertain plants has been studied in [28] and some recent developments in [23, 29].

3.2 Actuated part of the system

The control of the fully-actuated subsystem consists of a multivariable nonlinear time-invariant system, which has one output θ_3 and one input Γ_3. Feedback linearization is a very well-known nonlinear control technique. The core of the technique is to cancel out all the nonlinearities and impose the desired linear dynamics. In essence, it transforms the original system into an equivalent linear form by change of coordinates and

feedback. More information about this technique can be found in [15–17]. The application of this technique to the fully-actuated subsystem is straightforward just defining the torques for the inner loop of the articulated joints to cancel out all the nonlinearities as follows

$$\begin{aligned}\tau_{3n} := [M_{3n} - M_c^T M_{12}^{-1} M_c]\ddot{q}_{3n} + [C_{c2} - M_c^T M_{12}^{-1} C_{12}]\dot{q}_{12} \\ +[C_{3n} - M_c^T M_{12}^{-1} C_{c1}]\dot{q}_{3n} - M_c^T M_{12}^{-1} g_{12} + g_3 + M_c^T M_{12}^{-1}\tau_{12}.\end{aligned} \tag{10}$$

The subsystem (10) can be expressed as

$$\tau_{3n} = [M_{3n} - M_c^T M_{12}^{-1} M_c] \cdot v_3 + f(\underline{X}, \tau_{12}), \tag{11}$$

where $\underline{X} = [\theta_1, \theta_2, ..., \theta_n, \dot{\theta}_1, \dot{\theta}_2, ..., \dot{\theta}_n]$ and the fictitious control signals $v_3 = \ddot{\theta}_3$ acting as an outer loop. Upon considering that the whole state vector is measurable, then $\underline{X}$ and τ_{12} are known from the underactuated subsystem. Thus, the trajectory tracking controller that renders $q_{3n}(t) \to q_{3n}^*(t)$, is easily completed with an outer-loop linear controller, e.g. with double poles located at P as

$$v_k := \ddot{q}_k^* - 2p_k(\dot{q}_k - \dot{q}_k^*) - p_k^2(q_k - q_k^*), \quad k = 3, 4, ..., n. \tag{12}$$

4 Simulation and experimental verification

Although the control strategy proposed in the paper is evaluated in a prototype of a 3-DOF robotic manipulator, the control strategy is developed in a general form and it can be used for an n-link underactuated manipulator.

4.1 The manipulator prototype

In order to validate experimentally the proposed control strategy, a 3-DOF manipulator implementing the ankle, knee and hip joints of the robotic system has been developed. Figure 2 shows a picture of the prototype and the testbed, indicating the main components along with the link lengths. The prototype, built with customized actuators and an aluminum frame structure, has been designed to be as lightweight and slim as possible, inspired by the biomechanical features of birds. The passive joint at the base emulating the claw is built with a pair of igus ESTM-06-SL polymer bearings crossed by a 6 mm section shaft used as a support point (the branch of the bird), whose friction is practically negligible. The rotation angle θ_1 is measured at 500 Hz with an AMS 5047 magnetic encoder connected to the STM32 Nucleo microcontroller board through SPI (Serial Peripheral Interface). Two different actuators are employed in the knee and hip, according to the performance requirements for each joint. On the one hand, a zero-backlash actuator, weighting 70 grams and built with a Maxon EC20 flat brushless motor and a Harmonic Drive CSF5-100 gearbox, is used in the knee joint, providing a rated torque of 0.6 Nm and torque/current control at 200 Hz through the external ESCON 36/3 controller. The joint angle θ_2 is also measured with an AMS 5047 magnetic encoder through the same microcontroller board, that generates the PWM signal corresponding to the torque reference of the motor.

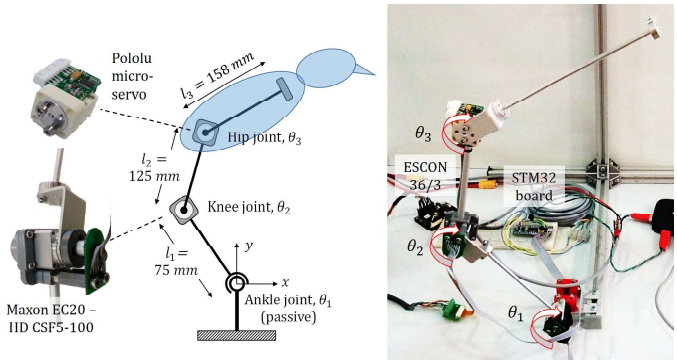

Fig. 2 The developed prototype.

On the other hand, the hip joint is built with a micro servo actuator (25 grams weight) based on a Pololu micro metal gear motor, integrating a Murata SV01 potentiometer to measure the angle θ_3, along with the low-level control electronics that communicate with the microcontroller board through a serial interface. This actuator, although more compact and lightweight than the other one, presents a lower performance in terms of rated torque (0.2 Nm), clearance (around 2 degrees), and positioning accuracy. Taking into account that the proposed control scheme applied in this particular case relies more on the knee that on the hip actuator to stabilize the passive joint, it is, therefore, more convenient to place the higher-performance actuator on the knee. Finally, the robotic system is controlled through the STM32 Nucleo board that interfaces with the computer where the control program is implemented through the serial interface, sending the torque references and feedback position measurements at 230400 bps. The firmware of the microcontroller was developed in C/C++ using the CubeMx IDE.

4.2 Simulated Results

Simulations have been carried out with the parameters of the prototype described in Section 4.1 to demonstrate the efficiency and robustness of the proposed technique. It has been considered that the mass of the links are concentrated at the joints and with values of $m_1 = 0.158$, $m_2 = 0.025$, and $m_3 = 0.0285$kg, and the length of the links are $l_1 = 0.075$, $l_2 = 0.125$, and $l_3 = 0.158$m. For the control of the fully-actuated subsystem, Bezier curves, which are smooth curves that can be differentiated indefinitely, have been chosen as reference trajectories. The dynamic model of the system is described by expression (1), making $n = 3$. The details about the mathematical model used in this work can be found in [30]. The results of the simulations are shown in Figure 3. The poles of the closed-loop system using the feedback control linearization in the actuated part are located at $p_3 = -15$. The GPI observer gain parameters used in the ADRC were set to: $\zeta_o = 1$, $\omega_o = 40$, $T_o = 40$. The controller design parameters of the ADRC were set to: $\zeta_c = 1$, $\omega_c = 25$. The initial point of the simulations and the equilibrium point used for implementing the ADRC control technique are $\theta_{10} = 110^\circ$, $\theta_{20} = -32.5^\circ$ and $\theta_{30} = -37.8^\circ$.

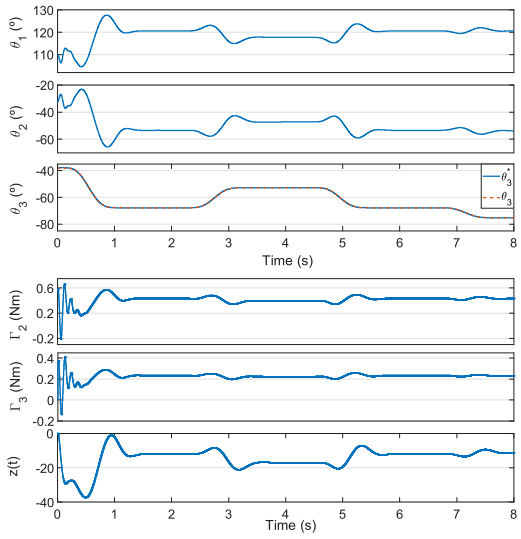

Fig. 3 Simulation results: angular coordinates and torques and estimation.

Figure 3 shows the trajectory tracking of the third joint, θ_3, that corresponds to the actuated part of the system. The results show that we achieve almost perfect trajectory tracking with the actuated part. Moreover, the position of the underactuated part of the system, θ_1 and θ_2 are also shown. The figure shows the positions that are needed to maintain the equilibrium of the system (around the unstable equilibrium point) while the third joint follows a preset trajectory. Figure 3 also shows the torques needed in joint 2 and joint 3 to control the system. Also, this figure shows the estimation of the perturbation that the GPI observer is estimating during the maneuver.

4.3 Experimental Results

Experiments have been performed with the robot manipulator described in Section 4.1 to show the effectiveness and robustness of the proposed control scheme in real applications. The poles of the closed-loop system using the feedback control linearization have been located at $p_k = -15$. The proposed ADRC controller is implemented and compared with the linear quadratic regulator (LQR). The GPI observer gain parameters used in the ADRC were set to: $\zeta_o = 1$, $\omega_o = 40$, $T_o = 40$. The controller design parameters of the ADRC were set to: $\zeta_c = 1$, $\omega_c = 5$. On the other hand, the LQR has been designed using the linear approximate model (3) and (4) at the equilibrium point ($\theta_{10} = -90^\circ$, $\theta_{20} = 0^\circ$), with weighting matrices $Q = 0.5 \cdot I$ and $R = 5 \cdot I$ (I is the identity matrix), yielding the controller gains $K = [-0.5463 \;\; -0.0298 \;\; -0.007 \;\; 0.0755]$. For the experiments with the real prototype, the control technique is implemented for the case that the system is hanging and we want to control the system around this stable equilibrium point. Figure 4 shows the angular coordinates of the robot manipulator for the cases: (a) controlling only the fully-actuated subsystem, i.e. no control on the underactuated one, (b) controlling the underactuated subsystem with the LQR and the fully-actuated one with the feedback linearization and (c) controlling the underactuated subsystem with the ADRC and fully-actuated one with the feedback linearization.

Figure 4 also shows the angular coordinate of the third joint, the preset trajectory is a sinusoidal signal during the first two seconds to exert a continuous disturbance in the underactuated part and validate the robustness of the ADRC. This angular coordinate is practically the same for the three cases showing the excellent performance of the feedback linearization for the three cases. Figure 4.d shows the trajectory tracking error in the three aforementioned cases. These experiments show good results in cases (b) and (c) because the controller of the fully-actuated subsystem was able to track the prescribed trajectories, while the underactuated system can stabilize the system around an equilibrium point. For that reason, the trajectory tracking error is reduced in these cases in comparison with the case of not using a control technique for the underactuated subsystem. Finally, the results also show that the proposed ADRC is much more efficient in reducing the trajectory tracking error than the LQR because the former estimates the coupling between the two subsystems and it can approximately cancel it.

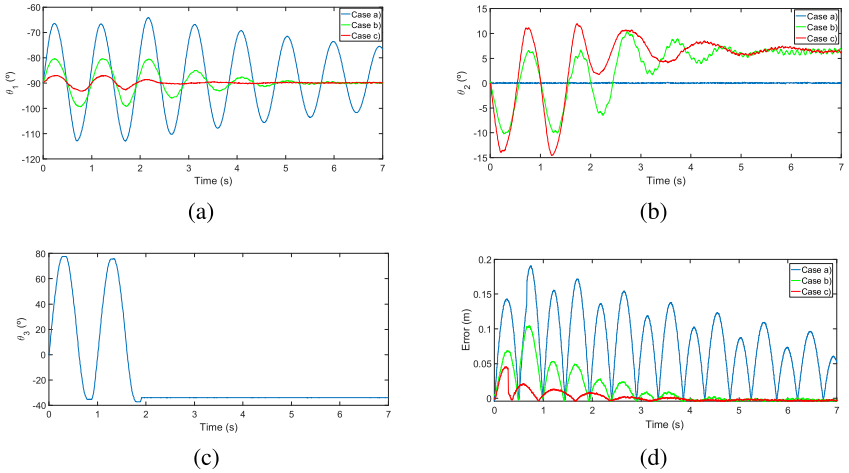

Fig. 4 Angular coordinate θ_1, θ_2, θ_3 and trajectory tracking errors.

5 Conclusions

This work presents an under-actuation model of a mechanical arm that imitates the birds having two-link legs, a body link, and two-link arms, being all active links except the first passive one. This model presents the behavior of a robotic bird, right before the take-off from a branch. The strategy of control approach includes two subsystems: a) the leg counterpart (under-actuated), which includes the two first links, and b) the body and arm subsystem (fully actuated) with the rest of the links. The control part of the fully-actuated links uses feedback linearization, and the under-actuated part, which is the difficult one, employs a linear high gain extended observer-based active disturbance rejection control approach which performs state/disturbances estimation. Although the setup is a three-DoF platform, the proposed methodology could be generalized for arms with more DoFs. The simulation results offer a more complicated under-actuated mechanism because it is controlled around an unstable equilibrium point. Experimental re-

sults demonstrate that the proposed control technique exhibits excellent behavior and it can estimate and reject the coupling between both subsystems. This technique is compared in experimentation with the well-known LQR method showing that the introduced control works efficiently for this kind of system and has a strong disturbance rejection ability in comparison with other methods.

ACKNOWLEDGMENT

The authors acknowledge support from the European Project GRIFFIN ERC Advanced Grant 2017, Action 788247; and also partially support from "Sistema robótico híbrido aéreo-acuático para muestreo, monitorización e intervención (HAERA)" funded by the Spanish Ministry of Science and Innovation PID2020-119027RB-I00.

References

1. Raphael Zufferey and et al. Design of the high-payload flapping wing robot e-flap. *IEEE Robotics and Automation Letters*, 6(2):3097–3104, 2021.
2. Wei Sun, Jingjun Yu, Guangping He, and Yueri Cai. Study on transmission mechanism and flexible flapping wings of an underactuated flapping wing robot. *J. Intell. & Robot Syst*, 104(2):1–13, 2022.
3. Raphael Zufferey, Jesus Tormo Barbero, Daniel Feliu Talegon, Saeed Rafee Nekoo, Jose Angel Acosta, and Anibal Ollero. How ornithopters can perch autonomously on a branch. *arXiv preprint arXiv:2207.07489*, 2022.
4. Jonathan Hoff and Joohyung Kim. Two-stage trajectory optimization for flapping flight with data-driven models. In *2021 IEEE Int. Conf. on Robots and Automat (ICRA)*, pages 7688–7692. IEEE, 2021.
5. Muhammad Labiyb Afakh, Terukazu Sato, Hidaka Sato, and Naoyuki Takesue. Development of flapping robot with self-takeoff from the ground capability. In *2021 IEEE Int. Conf. on Robots and Automat (ICRA)*, pages 321–327. IEEE, 2021.
6. Omuzi A Hudson, Mohamed Fanni, Sabah M Ahmed, and Ahmed Sameh. Bio-inspired jumping maneuver for launching flapping wing micro air vehicles. In *2018 IEEE International Conference on Autonomous Robot Systems and Competitions (ICARSC)*, pages 104–109. IEEE, 2018.
7. Zilong Zhang and C Steve Suh. Underactuated mechanical systems–a review of control design. *Journal of Vibration Testing and System Dynamics*, 6(01):21–51, 2022.
8. Rosana CB Rego and Fábio Meneghetti U de Araújo. Lyapunov-based continuous-time nonlinear control using deep neural network applied to underactuated systems. *Engineering Applications of Artificial Intelligence*, 107:104519, 2022.
9. Daniel Feliu-Talegon, José Ángel Acosta, and Anibal Ollero. Control aware of limitations of manipulators with claw for aerial robots imitating bird's skeleton. *IEEE Robotics and Automation Letters*, 6(4):6426–6433, 2021.
10. Daniel Feliu-Talegon, José Ángel Acosta, Alejandro Suarez, and Anibal Ollero. A bio-inspired manipulator with claw prototype for winged aerial robots: Benchmark for design and control. *Applied Sciences*, 10(18):6516, 2020.
11. Daniel Feliu, Jose Angel Acosta, Vicente Feliu, and Anibal Ollero. A lightweight beak-like sensing system for grasping tasks of flapping aerial robots. *IEEE Robotics and Automation Letters*, 2022.

12. Mark W Spong. The swing up control problem for the acrobot. *IEEE control systems magazine*, 15(1):49–55, 1995.
13. Xin Xin, Jin-Hua She, Taiga Yamasaki, and Yannian Liu. Swing-up control based on virtual composite links for n-link underactuated robot with passive first joint. *Automatica*, 45(9):1986–1994, 2009.
14. Ancai Zhang, Jianlong Qiu, Chengdong Yang, and Haibo He. Stabilization of underactuated four-link gymnast robot using torque-coupled method. *Int. Journal of Non-linear Mechanics*, 77:299–306, 2015.
15. Jean-Jacques E Slotine, Weiping Li, et al. *Applied nonlinear control*. Prentice hall Englewood Cliffs, NJ, 1991.
16. A. Isidori. *Nonlinear Control Systems*. Springer-Verlag, Berlin, 3rd edition, 1995.
17. S. Sastry. *Nonlinear Systems: Analysis, Stability and Control*. Springer-Verlag, New York, 1999.
18. Defeng Wu, Kexin Yuan, Youqiang Huang, Zhi-Ming Yuan, and Lisha Hua. Design and test of an improved active disturbance rejection control system for water sampling unmanned surface vehicle. *Ocean Engineering*, 245:110367, 2022.
19. Guolian Hou, Linjuan Gong, Mengyi Wang, Xiaodong Yu, Zhile Yang, and Xiaolin Mou. A novel linear active disturbance rejection controller for main steam temperature control based on the simultaneous heat transfer search. *ISA transactions*, 122:357–370, 2022.
20. Mario Ramirez-Neria, Z Gao, Hebertt Sira-Ramirez, Rubén Garrido-Moctezuma, and Alberto Luviano-Juarez. Trajectory tracking for an inverted pendulum on a cart: an active disturbance rejection control approach. In *2018 Annual American Control Conf. (ACC)*, pages 4881–4886. IEEE, 2018.
21. G Curiel-Olivares, J Linares-Flores, JF Guerrero-Castellanos, and A Hernández-Méndez. Self-balancing based on active disturbance rejection controller for the two-in-wheeled electric vehicle, experimental results. *Mechatronics*, 76:102552, 2021.
22. Shangjie Frank Ma, Ghazaale Leylaz, and Jian-Qiao Sun. Data-driven robust tracking control of underactuated mechanical systems using identified flat output and active disturbance rejection control. *International Journal of Control*, pages 1–17, 2021.
23. Carlos Aguilar-Ibañez, Hebertt Sira-Ramirez, and José Ángel Acosta. Stability of active disturbance rejection control for uncertain systems: A lyapunov perspective. *International Journal of Robust and Nonlinear Control*, 27(18):4541–4553, 2017.
24. Michel Fliess, Jean Lévine, Philippe Martin, and Pierre Rouchon. Flatness and defect of non-linear systems: introductory theory and examples. *International journal of control*, 61(6):1327–1361, 1995.
25. Shen Zhao and Zhiqiang Gao. An active disturbance rejection based approach to vibration suppression in two-inertia systems. *Asian Journal of Control*, 15(2):350–362, 2013.
26. M Ramírez-Neria, H Sira-Ramírez, R Garrido-Moctezuma, and Alberto Luviano-Juarez. Linear active disturbance rejection control of underactuated systems: The case of the furuta pendulum. *ISA transactions*, 53(4):920–928, 2014.
27. M Ramírez-Neria, H Sira-Ramírez, R Garrido-Moctezuma, and A Luviano-Juárez. Active disturbance rejection control of singular differentially flat systems. In *Society of Instrument and Control Engineers of Japan (SICE), 2015 54th Annual Conf. of the*, pages 554–559. IEEE, 2015.
28. Qing Zheng, L Gao, and Zhiqiang Gao. On stability analysis of active disturbance rejection control for nonlinear time-varying plants with unknown dynamics. In *Proceedings of the IEEE Conference on Decision and Control, New Orleans, LA, Dec*, pages 12–14, 2007.
29. Wenchao Xue and Yi Huang. Performance analysis of active disturbance rejection tracking control for a class of uncertain lti systems. *ISA transactions*, 58:133–154, 2015.
30. Xin Xin and Masahiro Kaneda. Swing-up control for a 3-dof gymnastic robot with passive first joint: design and analysis. *IEEE transactions on robotics*, 23(6):1277–1285, 2007.